Front. Energy 2021, 15(3): 621–630
https://doi.org/10.1007/s11708-021-0761-0

MINI REVIEW

Haoxuan MA, Chunli LIU

A mini-review of ferrites-based photocatalyst on application of hydrogen production

Abstract Photocatalytic water splitting for hydrogen production is a promising strategy to produce renewable energy and decrease production cost. Spinel-ferrites are potential photocatalysts in photocatalytic reaction system due to their room temperature magnetization, the high thermal and chemical stability, narrow bandgap with broader visible light absorption, and proper conduction band energy level with strong oxidation activity for water or organic compounds. However, the fast recombination of the photoexcited electrons and holes is a critical drawback of ferrites. Therefore, the features of crystallinity, particle size, specific surface area, morphology, and band energy structure have been summarized and investigated to solve this issue. Moreover, composites construction with ferrites and the popular support of TiO_2 or g-C_3N_4 are also summarized to illustrate the advanced improvement in photocatalytic hydrogen production. It has been shown that ferrites could induce the formation of metal ions impurity energy levels in TiO_2, and the strong oxidation activity of ferrites could accelerate the oxidation reaction kinetics in both TiO_2/ferrites and g-C_3N_4/ferrites systems. Furthermore, two representative reports of $CaFe_2O_4/MgFe_2O_4$ composite and $ZnFe_2O_4$/CdS composite are used to show the efficient heterojunction in a ferrite/ferrite composite and the ability of resistance to photo-corrosion, respectively.

Keywords photocatalyst, spinel-ferrite, composite, photocatalytic hydrogen production

Received Feb. 26, 2021; accepted Apr. 23, 2021; online Jul. 20, 2021

Haoxuan MA, Chunli LIU (✉)
Department of Physics and Oxide Research Center, Hankuk University of Foreign Studies, Yongin 17035, Republic of Korea
E-mail: chunliliu@hufs.ac.kr

Special Issue—Photocatalysis: From Solar Light to Hydrogen Energy (Guest Editors: Wenfeng SHANGGUAN, Akihiko KUDO, Zhi JIANG, Yuichi YAMAGUCHI)

1 Introduction

When hydrogen gas (H_2) is used as an energy source, only water will be produced after the combustion process. Therefore, H_2 has been considered as a potential candidate of renewable energy to relieve the energy crisis caused by limited fossil fuel resources and the detrimental impact on the environment. Several techniques have been developed to produce hydrogen gas, such as electrolysis, plasma arc decomposition, water thermolysis, thermochemical water splitting, thermochemical conversion of biomass, gasification, biofuel reforming, photovoltaic (PV) electrolysis, photocatalysis, and the photoelectrochemical method, etc [1,2]. Intensive research efforts have been made in each of these approaches to develop an optimized process in both environmental and economic respects.

The photocatalytic H_2 generation by water splitting is to use photocatalysts to induce the water splitting process as expressed in the Eq. (1) and generate H_2 as a reaction product [3]. TiO_2 is the first and the most widely investigated photocatalyst applied to photocatalytic water splitting [4]. Despite of its good stability and good efficiency, the main limitation of TiO_2 is imposed by its wide band gap energy (~3.2 eV). This band gap energy allows TiO_2 to only absorb light with the energy above the ultraviolet (UV) range, which only occupies 4% of solar energy spectrum [4]. Many different types of materials, including carbon nitrides, metal oxides, organic materials, etc. have been proposed and studied as candidates for promising high efficiency photocatalysts [5,6].

Ferrites (MFe_2O_4), such as $NiFe_2O_4$, $CoFe_2O_4$, etc., are iron oxide-based transition metal oxides with a spinel lattice structure. Ferrites have attracted much research attention as photocatalysts due to their suitable band gap energy around 2.0 eV for visible light absorption [7] and their room temperature magnetization for easy recollection [8,9]. Besides, different spinel ferrites could present various bandgaps and band positions [10]. More importantly, for water splitting generation of H_2, ferrites possess a good oxidation ability to promote the oxygen evolution

reaction (OER). During the OER process or the consumption of photoexcited holes, the valence state of metal M transforms to a high-valent species with a redox couple (the exchange of low and high valence state in the metal ions, for example, the redox couple of Ni^{2+}/Ni^{3+} during photocatalytic reaction). These redox couples are active species for oxidative reaction [11–13]. Hence, the stronger oxidation activity could accelerate the consumption holes or the whole redox reactions in a water splitting process. This activity could be expected in the water splitting H_2 production process to enhance the efficiency. Therefore, various ferrites and ferrite consisted composite materials have been reported for photocatalytic H_2 production.

In this paper, the reported results in ferrite-based photocatalysts applied in H_2 production by water splitting will be briefly reviewed. Moreover, the effect of synthesis methods, morphology, and microstructures on the H_2 production performance from several ferrites will be discussed first. Furthermore, ferrites/TiO_2 and ferrites/g-C_3N_4 composites will be presented to demonstrate the synergic effects from both materials in enhancing the light absorption and the separation of the photo-generated charge carriers.

2 Basic principle of photocatalytic hydrogen generation from water

Utilization of light energy on a semiconductor photocatalyst to split water and produce hydrogen is a multi-electron process as expressed in Eq. (1), which is also referred to as photoreduction.

$$2H_2O + 2e^- \rightarrow H_2 + 2OH^- \quad (1)$$

The required energy for the reduction process is 0 eV versus normal hydrogen electrode (NHE), at pH = 0. The electrons are provided from the semiconductor photocatalyst by light absorption. To induce the reduction of water, the electrons should possess a higher energy than that required for Eq. (1), i.e., the conduction band energy level of the semiconductor should be negative. At the same time, the photo-generated holes in the valence band participate in an oxidation process, including the generation of O_2 from water, or the oxidation of other chemicals used as scavenger [14,15]. The overall process of photoreduction of water to hydrogen is schematically demonstrated in Fig. 1 [16]. The process involves light irradiation (1), light absorption and excitation of electrons and holes to the conduction band (CB) and valence band (VB), respectively (2), migration of electrons and holes to reactive sites (3), reduction and oxidation reactions on the reactive sites (4). In addition, the recombination of photoinduced electrons and holes occurs through path (5)–inside the catalyst and (6)–on the surface of the catalyst, which are well known as the main factors limiting the photocatalytic efficiency.

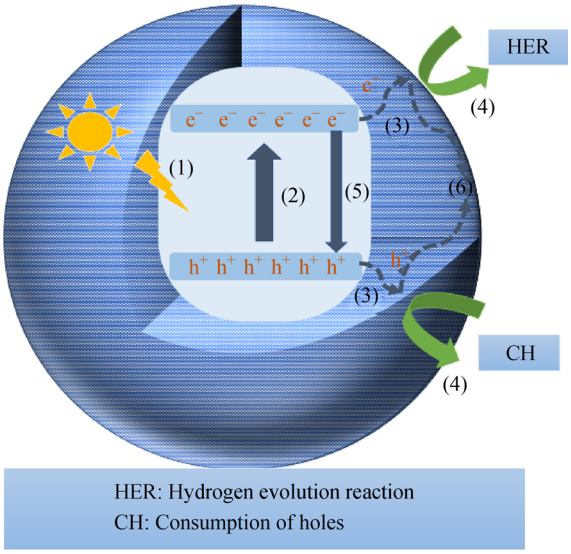

Fig. 1 Schematic of photocatalytic production of hydrogen.

Accordingly, the effective strategy to enhance the photocatalytic H_2 production is to reduce the charge recombination by inducing more migration paths for separation. Especially, a higher possibility for charges transferring to the surface of the photocatalyst, i.e., in step (3) of Fig. 1, can enable more charges to participate the redox reactions. In addition, since the water only can be adsorbed on the surface of the photocatalyst, the photocatalysts with a hydrophilic surface and large specific surface area are considered favorable. The photocatalytic production of hydrogen is mainly conducted in a liquid environment or an aqueous suspension state. Therefore, the recovery and collection of photocatalyst should be considered. Based on these requirements, it is obvious that the narrow bandgap energy and room temperature magnetization make ferrites suitable for photocatalytic H_2 generation.

3 Ferrite photocatalyst

3.1 Basic structure of spinel ferrite

The partial unit cell of spinel ferrite AB_2O_4 is depicted in Fig. 2. There are 8 A sites and 16 B sites in which the metal cations occupy the tetrahedral coordination (A) and octahedral coordination (B), respectively. Basically, when A sites are occupied by M^{2+} cations and B sites are occupied by Fe^{3+} ions, the ferrite is called a normal spinel. If the occupancies of A sites are completely coordinated with Fe^{3+} ions, it is called inverse spinel [17]. However, most of the ferrites display an intermediate state. Ferrites can exhibit several types of magnetism, and their magnetic behaviors are directly influenced and tuned by the distribution of the ions between A and B sites mentioned

above [18]. Most of the spinel ferrites are soft magnetic materials. They can be used as the magnetic-recoverable photocatalyst because they can be easily magnetized and demagnetized. According to the description of soft ferrites from Mathew et al. [19], the magnetic properties of soft ferrites are mainly induced by the interactions between some particular metallic ions with the oxygen ions. These interactions could create magnetic domains, which can be aligned in a magnetic field, resulting in a net magnetic response. The band gap energy could also be tuned by selecting the A^{2+} cation. Normally, the electronic structures or energy bands are mainly affected by the cationic characters and the corresponding d-d hybridized orbitals. A partially inverted structure by swapping an octahedral ion with a tetrahedral ion site could be used to adjust the net magnetic moments and electronic structures [18,20,21]. Therefore, the spinel ferrites could be easily collected by a magnet, which present several band energy features with different A and B sites, as shown in Figs. 3(a) and 3(b). However, the investigation of such tunning effect has rarely been reported in the application of photocatalytic reaction.

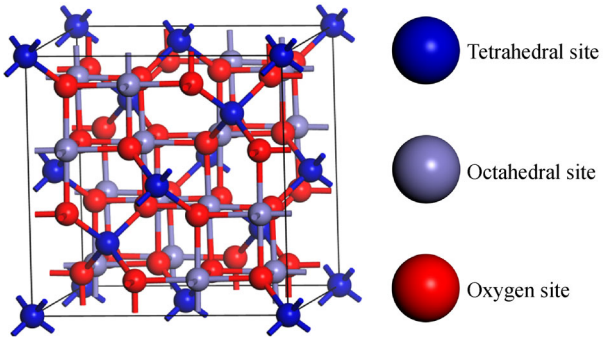

Fig. 2 Partial unit cell of spinel ferrite AB_2O_4.

3.2 Application in photocatalytic hydrogen production

Various individual spinel ferrites, such as $CoFe_2O_4$ [22], $NiFe_2O_4$ [21,32,33], $MgFe_2O_4$ [23,24], $CuFe_2O_4$ [25,26], and $ZnFe_2O_4$ [27–29] have been investigated for their hydrogen generation capability under solar irradiation.

Lopez et al. synthesized $CoFe_2O_4$ nanoparticles through coprecipitation and mechanical ball milling, and suggested that the high-density surface oxygen vacancies generated during the ball milling process improve the photocatalytic hydrogen production [22]. The surface oxygen vacancies presumably could enhance the water adsorption capacity of the material. The formation and effect of oxygen vacancies were also investigated in Refs. [30,31]. Peng et al. reported that the $NiFe_2O_4$ nanoparticles prepared through a hydrothermal and calcination process by using cetyltrimethylammonium bromide (CTAB) as a template directing agent presented much better performance of hydrogen evolution reaction (HER: 154.5 mol/(g·h) than $NiFe_2O_4$ aggregation (HER: 16.1 mol/(g·h) prepared without

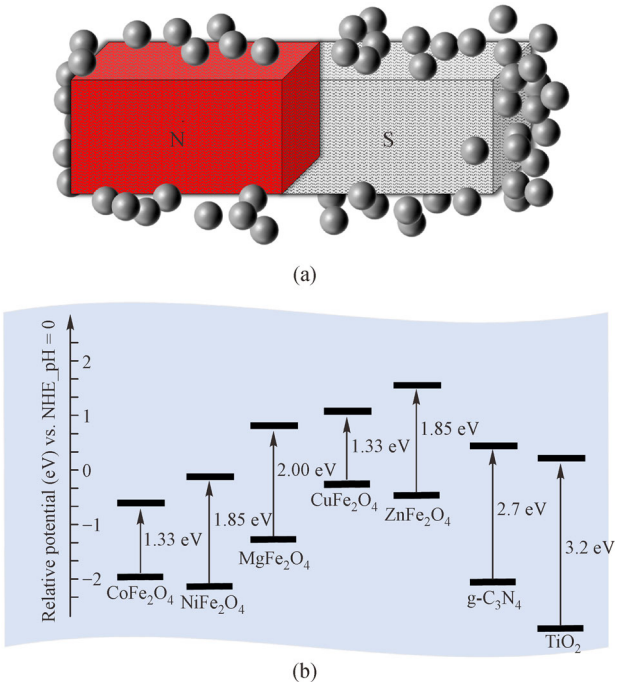

Fig. 3 Spinel ferrites easily collected by a magnet. (a) Easy collection of spinel-ferrites by a magnet (The gray balls are spinel ferrites nanoparticles.); (b) relative energy diagrams for MFe_2O_4 (M = Co, Ni, Mg, Cu, and Zn).

adding CTAB [32]. The authors attributed the improved photocatalytic efficiency to the relative larger surface area and small particle size in well dispersed $NiFe_2O_4$ nanoparticles. Hong et al. prepared high crystalline mesoporous $NiFe_2O_4$ by using an aerosol spray pyrolysis method (ASPM) with a structure directing agent of Pluronic F127 [33]. Their results further clarified the importance of a larger surface area and crystallinity through comparing amorphous and well-crystallized $NiFe_2O_4$ with a similar morphology and size. Rekhila et al. also demonstrated the stability of $NiFe_2O_4$ in an aqueous media and under illumination during the photocatalytic hydrogen production process [21]. Guzmán-Velderrain et al. synthesized $MgFe_2O_4$ nanoparticles through a coprecipitation combined with hydrothermal treatment to keep the particles in a nanometric size [23]. A higher activity in photocatalytic hydrogen production of $MgFe_2O_4$ than TiO_2 was demonstrated, which was attributed to the more efficient visible light absorption in $MgFe_2O_4$. Zazoua et al. reported the synthesis of $MgFe_2O_4$ nanoparticles with a diameter of approximately 1.8 nm and a specific surface area above 60 m^2/g through layered double hydroxides [24]. Accordingly, the enlarged surface area induced a desired photocatalytic hydrogen production. Saadi et al. performed photoelectrochemical (PEC) studies on the hydrogen production property of CuM_2O_4 (M: Co, Fe, Al, Mn, and Cr) [25], the p type $CuFe_2O_4$ and $CuCo_2O_4$ presented a great promise as H_2-photocathodes. In addition, the $CuFe_2O_4$ synthesized via a citric acid

assisted sol-gel method had more uniform nanoparticles with a diameter of 80 nm and larger specific surface areas, as compared to those obtained from solid-state reaction and co-precipitation [26]. It is proposed that the larger surface area enables the photocatalysts to adsorb more photons, and the smaller crystalline size can provide a shorter traveled path and consequently a longer lifetime for the photocarriers. The oxalic acid is shown to be a promising sacrificial reagent for holes because its strong reductive ability could promote the consumption of photoinduced holes and enhance the separation of photoexcited electron/hole pairs. Lv et al. produced floriated $ZnFe_2O_4$ nanostructures constructed by porous nanorods with an average length of 122 nm and a diameter of 29 nm via a mild hydrogen thermal and thermal decomposition process, in the presence of CTAB as a template-directing reagent [27]. In comparison with flaky $ZnFe_2O_4$, floriated $ZnFe_2O_4$ presented an enhanced activity. It was attributed to the small crystalline size and special rod structure that are beneficial for the transfer and separation of the photo-induced carriers. Besides, the nanorods and mesoporous structure were favorable for releasing the CO_2 produced from the oxidation of sacrificial reagent of methanol, which further promote the efficiency of hydrogen production. Dom et al. prepared highly crystalline $ZnFe_2O_4$ nanoparticles with a crystallite size of 35 nm using a rapid microwave irradiation method [28], and confirmed that a good crystallinity and a reduced particle size are beneficial for photocatalytic hydrogen generation. Recently, Rodriguez-Rodriguez et al. synthesized $CoFe_2O_4$, $NiFe_2O_4$, and $ZnFe_2O_4$ by utilizing a novel oil-in-water microemulsion method and compared their performance in photocatalytic hydrogen production [29]. $ZnFe_2O_4$ had the best performance, mostly due to more favorable electronic band positions as illustrated in Fig. 1(a). The more negative conduction band energy (–1.65 eV versus NHE) than other ferrites endorses $ZnFe_2O_4$ a stronger reduction force to promote the water splitting process.

The above literature review indicates that spinel ferrites can be used for hydrogen production through the photocatalytic water splitting reaction. The main factors that affect the hydrogen production efficiency, such as crystallinity, particle size, specific surface area, morphology, and bandgap structure, are collected in Table 1. Although it seems not meaningful to compare the efficiency between the study of different groups due to the different setups, the comparison in individual study could provide a clear guidance for the design of the spinel ferrite to be used in photocatalytic hydrogen generation. In addition, the stability and reusability are important for photocatalytic applications. In ferrite-based photocatalysts, the reusability is mainly attributed to the retrievability of the photocatalysts by using a magnet [34], and the stability

Table 1 Summary of morphology, particle or crystalline size, crystallinity, and specific surface areas with corresponding HER properties

Materials/keywords	Method	Morphology	Particle size (crystalline size)	Surface area /($m^2 \cdot g^{-1}$)	HER /($mol \cdot g^{-1} \cdot h^{-1}$)
$CoFe_2O_4$ [22]/oxygen defects	Coprecipitation	Nanoparticles	25(20);	20.0	310.0
	Mechanical ball milling	Agglomerates	100–500(5)	4.0	490.0
$NiFe_2O_4$ [32]/surface area and size	Hydrothermal and calcination (CTAB)	Nanoparticles	(18.1)	76.0	154.5
	Hydrothermal and calcination	Agglomerates	(18.1)	smaller	16.1
$NiFe_2O_4$ [33]/crystallinity	ASPM	Mesoporous sphere	200 High crystallinity	121.0	44.0
	ASPM	Mesoporous sphere	200 Low crystallinity	278.0	9.0
$MgFe_2O_4$ [23]	Hydrothermal	Cubic	90	53.0	81.0
$CuFe_2O_4$ [26]/size	Sol-gel	Nanoparticles	80	–	1720.0
	Coprecipitation	Irregular particles	Irregular size	–	1333.0
	Solid state	Aggregate badly	1000	–	1060.0
$ZnFe_2O_4$ [27]/morphology	Hydrothermal and calcination	Porous nanorod	Length: 122 Diameter: 29	52.0	47.0
	Hydrothermal and calcination	Flaky	–	51.0	17.0
$ZnFe_2O_4$ [28]/size	Rapid microwave solid-state	Nanoparticles	(35)	4.6	133.4
	Solid-state	Agglomerates	(53)	2.2	31.7
$ZnFe_2O_4$	Oil-in-water microemulsion reaction	Nanoparticle	12–20	49	44.3
$CoFe_2O_4$	Same	Nanoparticle	12–20	64	16
$NiFe_2O_4$ [29] /band structures	Same	Nanoparticle	12–20	65	16.1

of lattice structure is due to the existence of the Fe ions [13]. Jia et al. compared the X-ray diffraction (XRD), X-ray photoelectron spectroscopy (XPS) and FTIR spectrometer (FTIR) results before and after the photocatalytic reaction to demonstrate the good stability of $CoFe_2O_4$ [34]. Rekhila et al. demonstrated the remarkable corrosion stability of $NiFe_2O_4$ in an aqueous media [21]. The corrosion rates are 752 μm/a and 1427 μm/a under dark and light irradiation, respectively, indicating that $NiFe_2O_4$ has a very stable semiconductor property.

4 Ferrite based composite photocatalysts for hydrogen generation

Although spinel ferrites can be used alone as photocatalysts, the efficiency needs to be improved for practical applications. It is well known that the recombination of photo-induced electron/hole pairs is one of the dominant reasons for the low photocatalytic activity in single material. In this vein, spinel ferrites-based composite photocatalysts have been reported with different compositions for water splitting hydrogen production. As exhibited in Fig. 4, various types of heterojunctions (I and II) between two semiconductors can be designed to promote the electron/hole separation. In this section, the performance of selected composite photocatalysts, mainly composed of ferrites with g-C_3N_4 or TiO_2, will be discussed. The preparation procedure, morphology, and hydrogen production rate are listed in Table 2.

4.1 TiO_2/ferrites

TiO_2 is the first and literally the mostly studied semiconductor photocatalyst, since its photocatalytic effect was reported for the photo-electrolysis of water in 1972 [4]. To overcome the limited solar light absorption due to the wide band gap energy of TiO_2 and the relatively high rate of recombination of electrons and holes, various modification approaches have been reported, including doping, surface modification, facet and morphology control, and formation of heterojunctions [35].

Composites which consisted of TiO_2 and ferrite materials can have the advantages of enhanced visible light absorption and easy magnetic retrievability, due to the relatively narrow band gap and room temperature magnetization in most ferrite nanoparticles. Most earlier studies applied TiO_2/ferrite composites to the degradation of aqueous pollutants [36–41]. In the work of Haw et al., the 3D urchin-like TiO_2 microparticles were hydrothermally synthesized and decorated with $CoFe_2O_4$ magnetic nanoparticles (NPs) via the co-precipitation method [36]. The designed composite presented much improved performance of photodegrading methylene blue due to the lower recombination rate of the photoexcited charge carriers (pseudo-first order rate constant k/h: 0.7432 (produced composite) > 0.2605 (synthesized 3D urchin-like TiO_2) > 0.1073 (commercialized rutile TiO_2) > 0.0321 (synthesized $CoFe_2O_4$)). Ghosh and Gupta synthesized $CoFe_2O_4/TiO_2$/rGO (rGO: reduced graphene oxide) through the co-precipitation method, in which it is proposed that the photo-generated electrons transfer easily from CB of TiO_2 to rGO via $CoFe_2O_4$, leading to an effective spatial separation of the electrons and holes. As a result, the suppressed charge recombination led to an improved performance in the photodegradation of chlorpyrifos, methyl orange, methylene blue, and rhodamine B [37,38]. Furthermore, Wei et al. synthesized a S-N doped $CoFe_2O_4$/rGO/TiO_2 nanocomposite via the facial vapor-thermal method. The S and N dopant created new defect energy levels to decrease the bandgap of TiO_2. The defects cannot only improve the light adsorption, but also improve the separation of photoexcited electrons and holes [39]. The presence of $CoFe_2O_4$ granted the above mentioned composite photocatalysts with the magnetic recoverable feature.

The promising photocatalytic properties of TiO_2/ferrite composites promoted their applications in photocatalytic

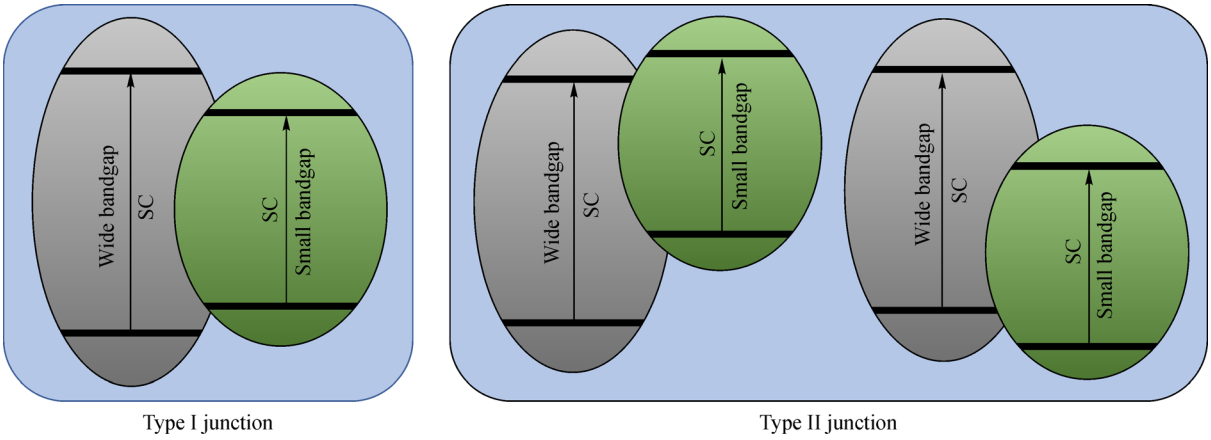

Fig. 4 Normal types (I and II) of junction between two semi-conductors (SC).

hydrogen production. Hafeez et al. synthesized a magnetically separable reduced graphene oxide-supported $CoFe_2O_4$-TiO_2 photocatalyst via the simple ultrasound-assisted wet impregnation method. It has been found that the integration of $CoFe_2O_4$ with TiO_2 could induce the formation of Ti^{3+} sites or substitution of Ti^{4+} by Fe^{3+} and Co^{2+}, which could induce the impurities or defects energy band levels and reduce the optical bandgap of TiO_2 from 3.2 to 2.8 eV, as shown in Figs. 5(a) and 5(b) [42,43]. Additionally, the induced defect levels cause the photo-induced electron in the conduction band to move to these extra levels before returning to the valance band, leading to the suppression of electron-hole recombination and increased photocatalytic performance (HER in $mol/(g \cdot h)^{-1}$: 16673 ($TiO_2/CoFe_2O_4$) > 5336 (TiO_2)) [43]. Similar observation was also reported for $CuFe_2O_4$-TiO_2/rGO composite from the same group [44]. The hydrogen production rate was improved (see Table 2) due to a double charge separation, i.e., the photoinduced electrons transfer from $CuFe_2O_4$ to TiO_2, then to rGO. Since the CB edge position of $CuFe_2O_4$ is more negative than that of TiO_2, the electron transfer direction is different from that in the case of $CoFe_2O_4/TiO_2$ composite. Interestingly, Kim et al. constructed a $NiFe_2O_4/TiO_2$ core/shell structure and achieved a good hydrogen productivity [45]. Since the band energy levels of $NiFe_2O_4$ are included in the range of TiO_2, the mechanism of charge transfer was described as follows: the photoexcited electrons from the conduction band of TiO_2 shell moved on the surface of the shell and fall into the conduction band of the $NiFe_2O_4$ core, then the excess accumulated electrons fall into the valence band of $NiFe_2O_4$ and TiO_2, and be excited to the conduction band again, which accordingly form a full flow cycle of the charge carriers. Consequently, $NiFe_2O_4$ can be considered as a co-catalyst to promote the separation of photoexcited electrons and holes, leading to an improved photocatalytic performance. It is obvious that due to the different band energy levels in each ferrite, the photoinduced carriers would flow in different pathways between ferrites and TiO_2. The injection of the impurity level of metal ions to TiO_2 is also a special feature coming from ferrites. On the other hand, it should be mentioned that despite the favorable effect of ferrite/TiO_2 composite, more systematic experimental and theoretical investigation on the charge migration mechanism and photocatalytic mechanisms are desired.

4.2 g-C_3N_4/ferrites

g-C_3N_4 is a typical polymer semiconductor that has been recently discovered to have promising properties as photocatalysts [46]. Wang et al. first discovered the photocatalytic water splitting evolution over g-C_3N_4 in 2009 [47]. g-C_3N_4 has attracted intensive research attention due to its suitable bandgap energy (2.7 eV), easy preparation with low cost, good chemical stability, and non-toxicity [48]. Additionally, the C and N atoms hybridize with the sp^2 orbital to form a highly delocalized π conjugated layer structure, which guarantees a high specific surface area [49]. However, when used alone, the insufficient visible light absorption, and especially the high recombination rate of the photogenerated electron-hole pairs, limit the photocatalytic activity of g-C_3N_4. The easy synthesis process, layered morphology, and the surface functional groups of g-C_3N_4 provide advantages in forming a well-contacted interface when used in heterojunction photocatalysts. In addition, the graphite like structure could support the growth of inorganic nanoparticles with a controlled size [50,51]. The combination of ferrites with g-C_3N_4 has been shown to effectively enhance the hydrogen production in water splitting.

Chen et al. reported the improved photocatalytic efficiency through coupling $MgFe_2O_4$ to g-C_3N_4/Pt [52]. Because the bandgap energy of $MgFe_2O_4$ is 2.0 eV (< 2.7 eV), and the conduction band edge position is more positive than that of g-C_3N_4, the $MgFe_2O_4$/g-C_3N_4 heterojunction could be regarded as the type I band alignment (Fig. 4), and the recombination of electrons and holes may not be quite effective. However, the authors found that the loading of Pt on g-C_3N_4 surface can prevent the migration of electrons from g-C_3N_4 to $MgFe_2O_4$ because the electrons can be easily accepted by Pt nanoparticles. Accordingly, the photocatalytic hydrogen production rate was improved by 100 times (up to 300.9 $mol/(g \cdot h)$) due to Pt induced charge separation. To investigate the advanced catalytic oxidation abilities of $MgFe_2O_4$, the linear sweep voltammetry (LSV) measurement was applied to study their electrocatalytic oxidation activities in oxygen evolution reaction. The results presented a lower onset potential of $MgFe_2O_4$/g-C_3N_4 than g-C_3N_4. It was concluded that $MgFe_2O_4$ cannot only extract the photoinduced hole from g-C_3N_4 to accelerate the charge transfer between $MgFe_2O_4$ and g-C_3N_4, but also act as an oxidative catalyst accelerating the oxidation reaction kinetics at g-C_3N_4 surface, as shown in Fig. 5(c) [52]. Similar characterizations have also been performed for $CoFe_2O_4$ and $NiFe_2O_4$ coupled with g-C_3N_4/Pt, and the results demonstrated that ferrites promote the separation of photoexcited electrons as well as possessing a superior surface oxidative catalytic activity. However, although both heterojunctions form a type II band alignment, the more negative VB edge position of $CoFe_2O_4$ relative to g-C_3N_4 supports a stronger driving force for the hole transfer from g-C_3N_4 to $CoFe_2O_4$ than in the case of g-C_3N_4/$NiFe_2O_4$. Therefore, the $CoFe_2O_4$/g-C_3N_4/Pt composite had a better performance than $NiFe_2O_4$/g-C_3N_4/Pt [53]. Recently, Aksoy et al. made a comparison of the photocatalytic hydrogen production activity among several types of ferrites (MFe_2O_4, M: Mn, Fe, Co, and Ni) coupled with g-C_3N_4 and found that $NiFe_2O_4$/mesoporous carbon nitride (mpg-CN) exhibited the best performance (Table 2) [54]. It is suggested that the better efficiency in $NiFe_2O_4$

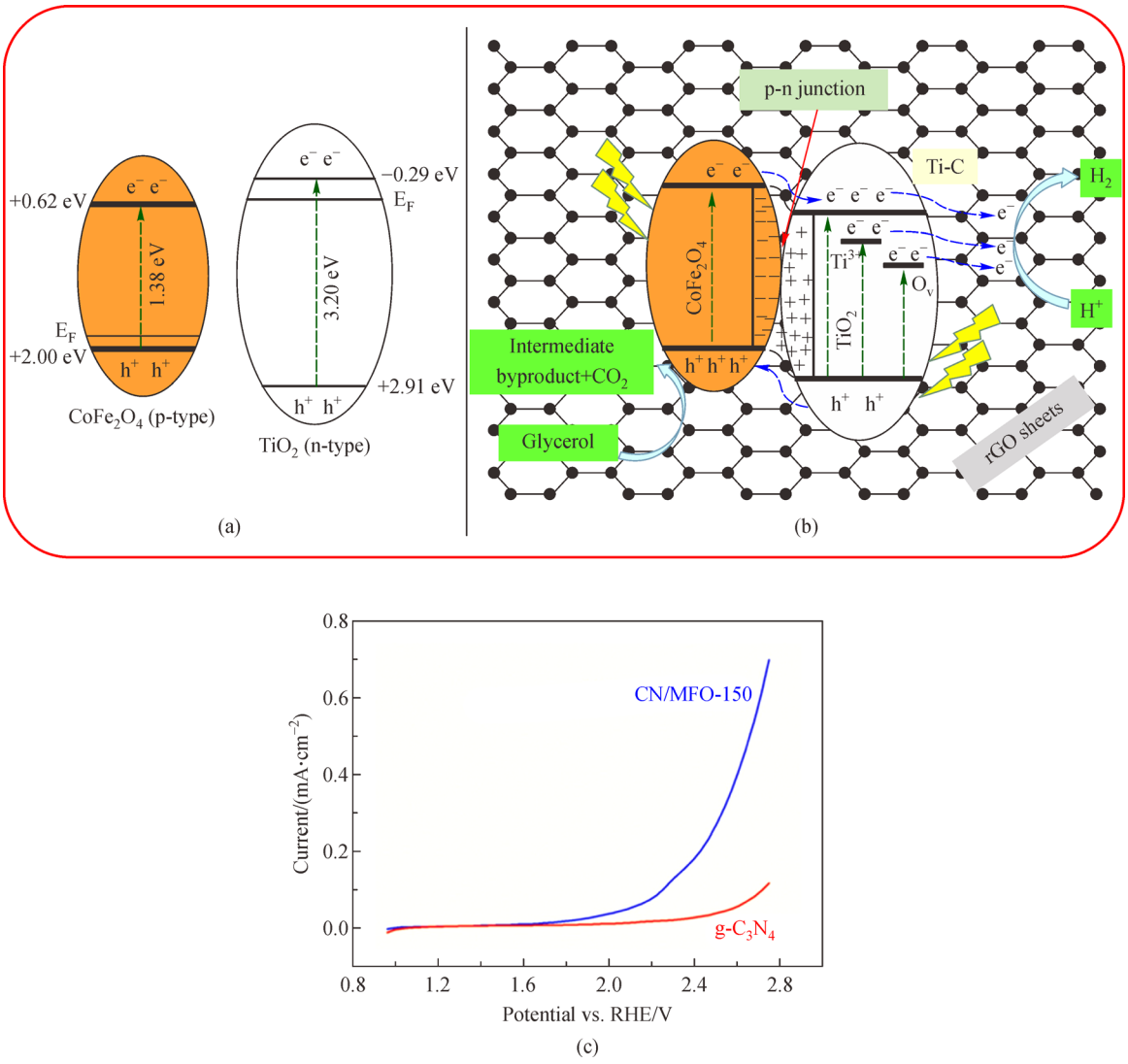

Fig. 5 Plausible mechanism of photocatalytic activity under UV-visible light (UV-Vis) irradiation of $CoFe_2O_4$-TiO_2/rGO photocatalyst. (a) Before contaction; (b) after contaction; (c) linear scan voltammogram curves for g-C_3N_4 and g-C_3N_4/$MgFe_2O_4$-150 (CN/MFO-150) electrodes.

may be explained by considering Ni as a good candidate for hydrogen evolution reaction catalyst due to its compact orbitals and low binding energy between hydrogen (1s orbital) and nickel (d orbital). The different morphology of $NiFe_2O_4$ nanoparticles (concave shape) as compared with other ferrites (spherical) should also be considered. It should be mentioned that although the oxidation ability of ferrites can be of advantage in enhancing the hydrogen generation, hole scavengers are normally necessary in promoting the production of hydrogen for most ferrite-based composites [54].

4.3 Other ferrite composites

In addition to the popular composites of ferrites/TiO_2 and ferrites/g-C_3N_4, here two representative reports of ferrites composites are also listed. A sufficient charge transfer ability could promote the photocatalytic performance in a composite system. Kim et al. fabricated a bulk heterojunction of $CaFe_2O_4$/$MgFe_2O_4$ by using the simple polymer complex method [55]. The $CaFe_2O_4$ and $MgFe_2O_4$ phases formed an interpenetrating network on a nanometer scale in a particle, which contained many randomly mixed and interfacing 20–30 nm particles. The photogenerated carriers in each phase could easily diffuse to the interface and be separated, due to the similar diffusion length of carriers with the domain size in either phase and sufficient contact at the interface. The composite supported with co-catalysts of RuO_2 and Pt had a quite high quantum yield for hydrogen evolution of 10.1% and 82.7 mol/(g·h) under visible light irradiation (450 W W-Arc lamp with UV cut-off filter, wavelength > 420 nm). This work provides a guidance for fabricating a highly efficient photocatalyst configuration with bulk heterojunctions. A proper energy

Table 2 Summary of performances in composites of TiO_2/ferrites and CN/ferrites

Materials	Synthesis methods	Morphology	HER/(mol·g^{-1}·h^{-1})	Lamp	Ref.
TiO_2	Ultrasound-assisted wet impregnation method (composite)	Non-special	5336	UV-Vis	[43]
TiO_2/rGO			9421		
$TiO_2/CoFe_2O_4$			16673		
$TiO_2/CoFe_2O_4$/rGO			76559		
TiO_2	Ultrasound-assisted wet impregnation method (composite)	Non-special	4640	UV-Vis	[44]
TiO_2/rGO			9397		
$TiO_2/CuFe_2O_4$			14719		
$TiO_2/CuFeO_4$/rGO			35981		
TiO_2	Sol-gel/precipitation	Core/shell	0 mL	UV	[44]
$TiO_2/NiFe_2O_4$			18.5 mL		

Note: In addition to enhanced light absorption and separation of h^+/e^- pairs, ferrites could also induce the metal and oxygen defect levels in TiO_2 to further improve the photocatalytic activity.

Materials	Synthesis methods	Morphology	HER/(mol·g^{-1}·h^{-1})	Lamp	Ref.
g-C_3N_4 (CN)	Sol-gel /calcination	Non-special	12.5	Vis $>$420 nm	[52]
CN/Pt			100.0		
CN/$MgFe_2O_4$			3.0		
CN/$MgFe_2O_4$/Pt			300.9		
CN/Pt	Sol-gel /calcination	Non-special	53.7	Vis $>$420 nm	[53]
CN/$NiFe_2O_4$/Pt			161.1		
CN/$CoFe_2O_4$/Pt			187.9		
CN	Liquid self-assembly	Uniformly nano-ferrites	0.27	Vis $>$420 nm	[54]
CN/$MnFe_2O_4$			1.07		
CN/$CoFe_2O_4$			1.51		
CN/$NiFe_2O_4$			1.82		

Note: Different type of ferrites would induce different multi-step electron transfers in a composite with g-C_3N_4 due to different band energy alignments. Especially, the strong oxidation ability of ferrites would accelerate the hydrogen production in the composite of CN/ferrites.

level distribution in a composite can also be used to protect a certain component from being photo-corroded during the photocatalytic reaction. For example, the accumulated holes on the CdS will oxidize S^{2-} to S, resulting in an increased risk of photo-corrosion in CdS. In this vein, Yu et al. synthesized a composite of $ZnFe_2O_4$ decorated CdS nanorods through the solvothermal process [56]. The type II junction between $ZnFe_2O_4$ and CdS with a more negative conduction band level of $ZnFe_2O_4$ promotes the photoinduced electrons transfer from $ZnFe_2O_4$ to CdS, and the migration of holes occurs in the opposite direction, resulting in the CdS protection, electron/hole separation, and magnetic recyclability. Finally, the specific hydrogen evolution rate was achieved as 2.44 mmol/(g·h) with a much longer-term stability than CdS alone.

5 Conclusions

This paper briefly reviewed some of the ferrites and ferrite heterojunction composites (ferrite/TiO_2 and ferrite/g-C_3N_4) for photocatalytic hydrogen production from water splitting. In the case of ferrites, the special feature of magnetic property promotes the easier collection of catalyst from aqueous suspension by using the magnetic field. Various approaches, including control of crystallinity, particles size, specific surface area, and morphology, have been used to efficiently improve the separation of photoinduced electrons and holes. $ZnFe_2O_4$ seems to have the best photocatalytic activity among common ferrites due to its higher conduction band level which can provide a stronger driving force for the reduction of water. Ferrites-based composites, especially with TiO_2 and g-C_3N_4 are selected to review the photocatalytic hydrogen generation activity. Besides the convenient collection process, the addition of ferrites to TiO_2 could induce some impurity or defects energy levels to increase light absorption, and suppress the recombination of electron/hole pairs. In the case of ferrite/g-C_3N_4 composite, normally, the photocatalysts shows an enhanced light absorption and separation of the charge carriers, and the highly efficient surface oxidation ability of ferrites also lead to enhanced kinetic reactions of electrons and holes to H^+ ions and scavengers, respectively. However, even though the junction of ferrites-based composites could promote the efficient charges separation and magnetic recyclability etc., the low surface activity still limits the hydrogen evolution rate. Co-catalysts of noble metals or conductive carbonaceous materials are necessary to accelerate the kinetic reaction rate with water. Currently, to improve the surface reactivity and suppress the recombination of electrons and holes, most of the spinel-ferrites are loaded with noble metal nanoparticles of Pt and Au or graphene-based materials. Researchers can, in the future, investigate the synthesis and

performance of loading single atoms (Pt, Au, etc.) or nonnoble cocatalyst on ferrites with a low cost and a high surface activity. The built-in electric field induced by facets controlling is also worth exploring to improve the separation of charge carriers and study the reactivities to hydrogen evolution reaction. Besides, various composite systems can be investigated depending on the different features of virous ferrites. Moreover, according to the requirements of HER, a comprehensively theoretical study on the structures of different types of ferrites could be conducted, as there are few reports in this regard.

Acknowledgements This research was supported by the Basic Science Research Program (2019R1A2C1086881) through the National Research Foundation of Republic of Korea funded by the Ministry of Science, Information and Communications Technology (ICT) and Future Planning.

References

1. Dincer I, Acar C. Review and evaluation of hydrogen production methods for better sustainability. International Journal of Hydrogen Energy, 2015, 40(34): 11094–11111
2. Kalamaras C M, Efstathiou A M. Hydrogen production technologies: current state and future developments. Conference Papers in Science. Hindawi, 2013, available at the website of hindawi.com
3. Maeda K, Domen K. Photocatalytic water splitting: recent progress and future challenges. Journal of Physical Chemistry Letters, 2010, 1(18): 2655–2661
4. Fujishima A, Honda K. Electrochemical photolysis of water at a semiconductor electrode. Nature, 1972, 238(5358): 37–38
5. Navlani-García M, Mori K, Kuwahara Y, et al. Recent strategies targeting efficient hydrogen production from chemical hydrogen storage materials over carbon-supported catalysts. NPG Asia Materials, 2018, 10(4): 277–292
6. Fajrina N, Tahir M. A critical review in strategies to improve photocatalytic water splitting towards hydrogen production. International Journal of Hydrogen Energy, 2019, 44(2): 540–577
7. Bessekhouad Y, Trari M. Photocatalytic hydrogen production from suspension of spinel powders AMn_2O_4 (A = Cu and Zn). International Journal of Hydrogen Energy, 2002, 27(4): 357–362
8. Muthuselvam I P, Bhowmik R N. Structural phase stability and magnetism in Co_2FeO_4 spinel oxide. Solid State Sciences, 2009, 11 (3): 719–725
9. Brabers V A M. Progress in spinel ferrite research. In: Brück E, ed. Handbook of Magnetic Materials. Elsevier, 1995
10. Jia Y, Ma H, Zhang W, et al. Z-scheme $SnFe_2O_4$-graphitic carbon nitride: reusable, magnetic catalysts for enhanced photocatalytic CO_2 reduction. Chemical Engineering Journal, 2020, 383: 123172
11. Guo D, Kang H, Wei P, et al. A high-performance bimetallic cobalt iron oxide catalyst for the oxygen evolution reaction. CrystEngComm, 2020, 22(25): 4317–4323
12. Hong D, Yamada Y, Nagatomi T, et al. Catalysis of nickel ferrite for photocatalytic water oxidation using $[Ru(bpy)_3]^{2+}$ and $S_2O_8^{2-}$. Journal of the American Chemical Society, 2012, 134(48): 19572–19575
13. Xiong Y, Yang Y, Feng X, et al. A strategy for increasing the efficiency of the oxygen reduction reaction in Mn-doped cobalt ferrites. Journal of the American Chemical Society, 2019, 141(10): 4412–4421
14. Preethi V, Kanmani S. Photocatalytic hydrogen production. Materials Science in Semiconductor Processing, 2013, 16(3): 561–575
15. Bhatt M D, Lee J S. Nanomaterials for photocatalytic hydrogen production: from theoretical perspectives. RSC Advances, 2017, 7 (55): 34875–34885
16. Yang X, Wang D. Photocatalysis: from fundamental principles to materials and applications. ACS Applied Energy Materials, 2018, 1 (12): 6657–6693
17. Taffa D H, Dillert R, Ulpe A C, et al. Photoelectrochemical and theoretical investigations of spinel type ferrites ($M_xFe_{3-x}O_4$) for water splitting: a mini-review. Journal of Photonics for Energy, 2016, 7(1): 012009
18. Szotek Z, Temmerman W M, Ködderitzsch D, et al. Electronic structures of normal and inverse spinel ferrites from first principles. Physical Review. B, 2006, 74(17): 174431
19. Mathew D S, Juang R S. An overview of the structure and magnetism of spinel ferrite nanoparticles and their synthesis in microemulsions. Chemical Engineering Journal, 2007, 129(1–3): 51–65
20. Holinsworth B S, Mazumdar D, Sims H, et al. Chemical tuning of the optical band gap in spinel ferrites: $CoFe_2O_4$ vs $NiFe_2O_4$. Applied Physics Letters, 2013, 103(8): 082406
21. Rekhila G, Bessekhouad Y, Trari M. Visible light hydrogen production on the novel ferrite $NiFe_2O_4$. International Journal of Hydrogen Energy, 2013, 38(15): 6335–6343
22. Ortega López Y, Medina Vázquez H, Salinas Gutiérrez J, et al. Synthesis method effect of $CoFe_2O_4$ on its photocatalytic properties for H_2 production from water and visible light. Journal of Nanomaterials, 2015, 2015: 1–9
23. Peng T, Zhang X, Lv H, et al. Preparation of $NiFe_2O_4$ nanoparticles and its visible-light-driven photoactivity for hydrogen production. Catalysis Communications, 2012, 28: 116–119
24. Hong D, Yamada Y, Sheehan M, et al. Mesoporous nickel ferrites with spinel structure prepared by an aerosol spray pyrolysis method for photocatalytic hydrogen evolution. ACS Sustainable Chemistry & Engineering, 2014, 2(11): 2588–2594
25. Guzmán-Velderrain V, Meléndez Zaragoza M, et al. Photocatalytic hydrogen production under visible light over magnesium ferrite. In: XIV International Congress of the Mexican Hydrogen Society Cancun, Mexico, 2014
26. Zazoua H, Boudjemaa A, Chebout R, et al. Enhanced photocatalytic hydrogen production under visible light over a material based on magnesium ferrite derived from layered double hydroxides (LDHs). International Journal of Energy Research, 2014, 38(15): 2010–2018
27. Saadi S, Bouguelia A, Trari M. Photoassisted hydrogen evolution over spinel CuM_2O_4 (M = Al, Cr, Mn, Fe and Co). Renewable Energy, 2006, 31(14): 2245–2256
28. Yang H, Yan J, Lu Z, et al. Photocatalytic activity evaluation of tetragonal $CuFe_2O_4$ nanoparticles for the H_2 evolution under visible light irradiation. Journal of Alloys and Compounds, 2009, 476(1–2): 715–719
29. Lv H, Ma L, Zeng P, et al. Synthesis of floriated $ZnFe_2O_4$ with

porous nanorod structures and its photocatalytic hydrogen production under visible light. Journal of Materials Chemistry, 2010, 20 (18): 3665–3672

30. Dom R, Subasri R, Hebalkar N Y, et al. Synthesis of a hydrogen producing nanocrystalline $ZnFe_2O_4$ visible light photocatalyst using a rapid microwave irradiation method. RSC Advances, 2012, 2(33): 12782–12791
31. Rodríguez-Rodríguez A A, Moreno-Trejo M B, Meléndez-Zaragoza M J, et al. Spinel-type ferrite nanoparticles: synthesis by the oil-in-water microemulsion reaction method and photocatalytic water-splitting evaluation. International Journal of Hydrogen Energy, 2019, 44(24): 12421–12429
32. Zhang B Q, Lu L, Lai M O. Evolution of vacancy densities in powder particles during mechanical milling. Physica B, Condensed Matter, 2003, 325: 120–129
33. Geng Y, Ablekim T, Mukherjee P, et al. High-energy mechanical milling-induced crystallization in $Fe_{32}Ni_{52}Zr_3B_{13}$. Journal of Non-Crystalline Solids, 2014, 404: 140–144
34. Jia Y, Ma H, Liu C. Au nanoparticles enhanced Z-scheme Au-$CoFe_2O_4$/MoS_2 visible light photocatalyst with magnetic retrievability. Applied Surface Science, 2019, 463: 854–862
35. Singh R, Dutta S. A review on H_2 production through photocatalytic reactions using TiO_2/TiO_2-assisted catalysts. Fuel, 2018, 220: 607–620
36. Haw C, Chiu W, Abdul Rahman S, et al. The design of new magnetic-photocatalyst nanocomposites ($CoFe_2O_4$–TiO_2) as smart nanomaterials for recyclable-photocatalysis applications. New Journal of Chemistry, 2016, 40(2): 1124–1136
37. Gupta V K, Eren T, Atar N, et al. $CoFe_2O_4$@TiO_2 decorated reduced graphene oxide nanocomposite for photocatalytic degradation of chlorpyrifos. Journal of Molecular Liquids, 2015, 208: 122–129
38. Ghosh B K, Moitra D, Chandel M, et al. Preparation of TiO_2/cobalt ferrite/reduced graphene oxide nanocomposite based magnetically separable catalyst with improved photocatalytic activity. Journal of Nanoscience and Nanotechnology, 2017, 17(7): 4694–4703
39. Wei F, Wang H, Ran W, et al. Preparation of S–N co-doped $CoFe_2O_4$@rGO@TiO_2 nanoparticles and their superior UV-Vis light photocatalytic activities. RSC Advances, 2019, 9(11): 6152–6162
40. Yu Y Y, Zhang H Q. Reduced graphene oxide coupled magnetic $CuFe_2O_4$-TiO_2 nanoparticles with enhanced photocatalytic activity for methylene blue degradation. Chinese Journal of Structural Chiemistry, 2016, 35(3): 472–480
41. Jia Y, Liu J, Cha S, et al. Magnetically separable Au-TiO_2/nanocube $ZnFe_2O_4$ composite for chlortetracycline removal in wastewater under visible light. Journal of Industrial and Engineering Chemistry, 2017, 47: 303–314
42. Li C J, Wang J N, Wang B, et al. A novel magnetically separable TiO_2/$CoFe_2O_4$ nanofiber with high photocatalytic activity under UV–Vis light. Materials Research Bulletin, 2012, 47(2): 333–337
43. Hafeez H Y, Lakhera S K, Narayanan N, et al. Environmentally sustainable synthesis of a $CoFe_2O_4$–TiO_2/rGO ternary photocatalyst: a highly efficient and stable photocatalyst for high production of hydrogen (solar fuel). ACS Omega, 2019, 4(1): 880–891
44. Hafeez H Y, Lakhera S K, Karthik P, et al. Facile construction of ternary $CuFe_2O_4$-TiO_2 nanocomposite supported reduced graphene oxide (rGO) photocatalysts for the efficient hydrogen production. Applied Surface Science, 2018, 449: 772–779
45. Kim H S, Kim D, Kwak B S, et al. Synthesis of magnetically separable core@shell structured $NiFe_2O_4$@TiO_2 nanomaterial and its use for photocatalytic hydrogen production by methanol/water splitting. Chemical Engineering Journal, 2014, 243: 272–279
46. Wen J, Xie J, Chen X, et al. A review on g-C_3N_4-based photocatalysts. Applied Surface Science, 2017, 391: 72–123
47. Wang X, Maeda K, Thomas A, et al. A metal-free polymeric photocatalyst for hydrogen production from water under visible light. Nature Materials, 2009, 8(1): 76–80
48. Babu B, Koutavarapu R, Shim J, et al. Enhanced visible-light-driven photoelectrochemical and photocatalytic performance of Au-SnO_2 quantum dot-anchored g-C_3N_4 nanosheets. Separation and Purification Technology, 2020, 240: 116652
49. Wang S, He P, Jia L, et al. Nanocoral-like composite of nickel selenide nanoparticles anchored on two-dimensional multi-layered graphitic carbon nitride: a highly efficient electrocatalyst for oxygen evolution reaction. Applied Catalysis B: Environmental, 2019, 243: 463–469
50. Yousaf M U, Pervaiz E, Minallah S, et al. Tin oxide quantum dots decorated graphitic carbon nitride for enhanced removal of organic components from water: green process. Results in Physics, 2019, 14: 102455
51. Wang L, Si W, Tong Y, et al. Graphitic carbon nitride (g-C_3N_4)-based nanosized heteroarrays: promising materials for photoelectrochemical water splitting. Carbon Energy, 2020, 2(2): 223–250
52. Chen J, Zhao D, Diao Z, et al. Bifunctional modification of graphitic carbon nitride with $MgFe_2O_4$ for enhanced photocatalytic hydrogen generation. ACS Applied Materials & Interfaces, 2015, 7(33): 18843–18848
53. Chen J, Zhao D, Diao Z, et al. Ferrites boosting photocatalytic hydrogen evolution over graphitic carbon nitride: a case study of (Co, Ni) Fe_2O_4 modification. Science Bulletin, 2016, 61(4): 292–301
54. Aksoy M, Yanalak G, Aslan E, et al. Visible light-driven hydrogen evolution by using mesoporous carbon nitride-metal ferrite (MFe_2O_4/mpg-CN; M: Mn, Fe, Co and Ni) nanocomposites as catalysts. International Journal of Hydrogen Energy, 2020, 45(33): 16509–16518
55. Kim H G, Borse P H, Jang J S, et al. Fabrication of $CaFe_2O_4$/$MgFe_2O_4$ bulk heterojunction for enhanced visible light photocatalysis. Chemical Communications, 2009, (39): 5889–5891
56. Yu T H, Cheng W Y, Chao K J, et al. $ZnFe_2O_4$ decorated CdS nanorods as a highly efficient, visible light responsive, photochemically stable, magnetically recyclable photocatalyst for hydrogen generation. Nanoscale, 2013, 5(16): 7356–7360